MEASUREMENT OF PARAMETERS OF THE MOVING GAS BUBBLES WITH THE IMAGE TOMOGRAPH

Mariusz R. RZĄSA

Opole University of Technology, ul. Mikołajczyka 5, 45-271 Opole, Poland, m.rzasa@po.opole.pl

Abstract:
The paper presents an idea of a new measuring method based on image tomography. This method insists in registration of images of the moving bubbles from two perpendicular directions. Two images are used for determination of the center of mass, movement trajectory and local velocities. Volume and area of the bubble are defined by approximation of the bubble shapes by the known geometric figures. The paper also presents the algorithm of reconstruction of the bubble shapes and movement trajectories, as well as exemplary test results. The obtained results were compared with theoretical relationships published in literature.

Keywords: Image tomography, gas-liquid two-phase flow, algorithm of reconstruction, gas bubble measurement.

1. INTRODUCTION

Aeration is applied in many industrial processes, for example water aeration in biological treatment plants, solution of CO2 or other gases while chemical processes, or barbotage processes aiding chemical and mechanical processes, for example washing. Mass exchange between the liquid and the gas bubbles moving in it is an important element of such processes [1,2]. Effectiveness of the mass exchange is influenced by shapes and dimensions of the moving bubbles and the parameters of bubble movement [3]. The bubble volume, its area, movement velocity and movement trajectory are the most important parameters. The bubble movement trajectory must be usually be known because bubbles rarely move along the rectilinear paths.

Measurements of the moving bubbles are difficult from the metrological point of view [7, 8]. Determination of velocity of the gas bubble flow in a liquid is a very complicated problem from both theoretical and experimental point of view. There are numerous papers concerning that subject but there is no satisfactory solution of that problem. It results from a very complicated flow mechanism including rectilinear, zigzag or helical path of the bubble flow, depending on the flow conditions, rigid or free surface of the bubble, internal gas circulation in the bubble, different shapes of the flowing bubbles, interactions between the bubbles, effects occurring near the walls, the fluid velocity field flowing around the bubble.

Assessment of the bubble flow is often realized by visual observation in a transparent channel [4, 5, 6]. It is not easy to include an observed flow to the given structure and such decisions are usually subjective, so averaging distribution of phase concentration at time and space is often done by intuition.

At present, photographic methods joined with image analysis, or methods using process tomography [9, 10, 11] are more and more often applied for determination of gas bubble parameters. The paper presents a method using image tomography, which allows to determine both movement trajectories of the moving bubbles, and their local velocities and volumes as well.

2. IDEA OF THE MEASURING METHOD

The measuring system is based on image tomography using photographic methods joined with image analysis. A method of determination of the bubble movement trajectory was elaborated in order to determine the spatial velocity distribution. The trajectory is determined on the basis of video images obtained from the flow over-exposure from two perpendicular directions (Fig.1).Then, image of the moving bubbles is reconstructed. Successive image frames allow to determine a sense and a value of the velocity vector of the moving bubble, and, in a consequence, it is possible to define the movement trajectory. Volume and area are calculated by approximation of the bubble shapes with the known geometric figures.

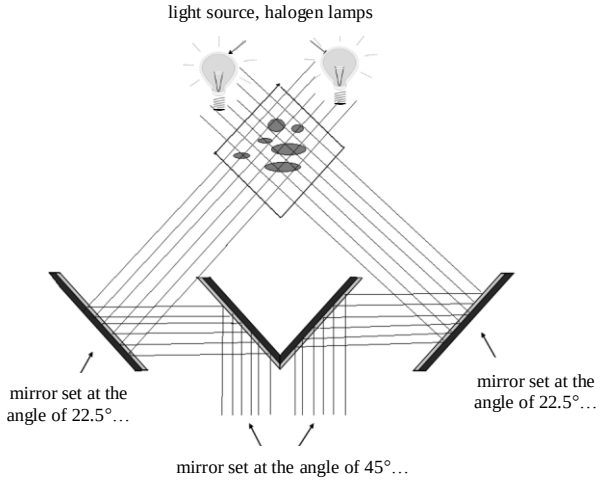

Fig. 1: Principle of image tomograph operation.

A system of mirrors was elaborated in order to obtain the column images from two sides, synchronized at time. The mirrors allow to register the image with one camera. This solution does not require image synchronization, so reconstruction becomes easier.

3. THE IMAGE RECONSTRUCTION ALGORITHM

Fig.2 shows a typical image of a flow, registered by a camera of the image tomograph. Velocities of the moving bubbles are strongly different. While a flow, bubbles often join together, or divide into some smaller ones, and then reconstruction becomes more difficult.

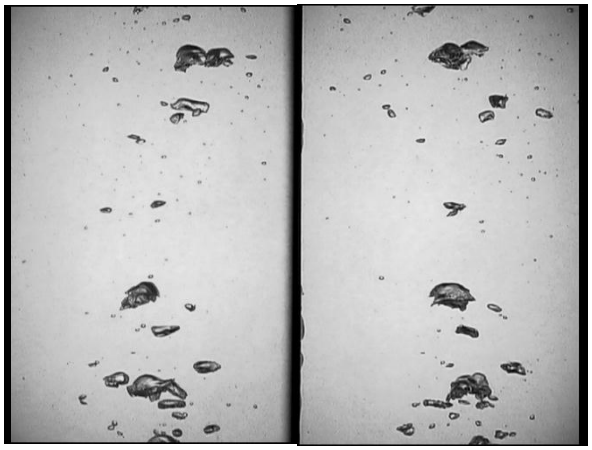

Fig. 2: Typical flow image from the optical tomograph.

The reconstruction algorithm includes some stages. The first stage includes isolation of the objects from the image and their segregation, next their positions are determined according to analysis of the successive image frames. The considered image has been converted into the binary form (Fig.3). The binary conversion of image is described in [12].

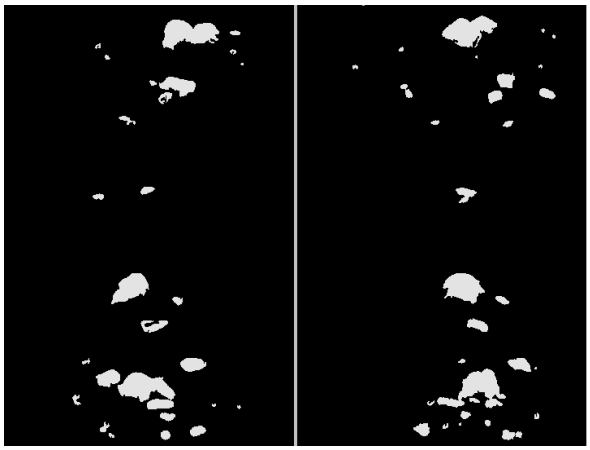

Fig. 3: Image after binary conversion.

3.1 Determination of bubble velocity and trajectory

A shape of the moving bubble often changes, so the point in relation to which the path travelled by the bubble is determined is assumed as the centre of mass. Since the tomograph gives us two images of the bubble observed from two sides, the centre of mass is determined for each image separately (Fig.4), and coordinates of the centre of mass x_c and y_c are calculated from:

$$x_c = \frac{\sum A_p x_i}{\sum A_p} \qquad y_c = \frac{\sum A_p y_i}{\sum A_p} \tag{1}$$

where: A_p – area of one pixel of the image, x_i, y_i – value of the coordinate of *I-th* pixel.

The centres of mass for two bubble images along the *Z* axis can be a little different, so the following averaged value was assumed for z_x and z_y.

$$z = \frac{z_x + z_y}{2} \tag{2}$$

where: z_x – coordinates of the centre of mass for the *XZ* projection plane, z_y – coordinates of the centre of mass for the *YZ* projection plane.

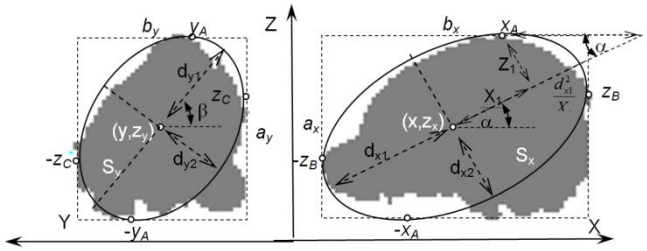

Fig. 4: View of the bubble image after binary conversion

Velocity of the moving bubble is determined on the basis of the shift vector in successive image frames with constant time between frames. Velocity is calculated from the following relationship:

$$v_g = \frac{\sqrt{(x_n + x_{n-1})^2 + (y_n + y_{n-1})^2 + (z_n + z_{n-1})^2}}{t_k} \tag{3}$$

where: x_n, y_n, z_n – coordinates of the centre of mass for n-1 image frame, x_{n-1}, y_{n-1}, z_{n-1} – coordinates of the centre of mass for n-1 image frame, t_k – time between the successive image frames.

3.2 Bubble shape reconstruction

Reconstruction insists in approximation of the bubble shape with ellipsoid (Fig.5). In order to determine the ellipsoid diameters it is necessary to define the points of contact (*A, B, C*) of the ellipsoid with sides of the prism circumscribed on the ellipsoid.

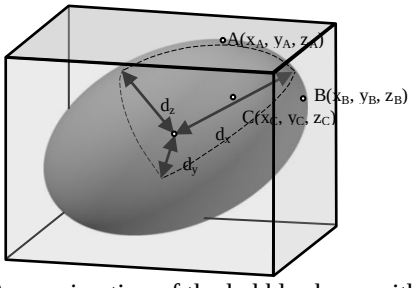

Fig. 5: Approximation of the bubble shape with ellipsoid.

Reconstruction begins from determination of coordinates of points of contact of the ellipsoid with sides of the prism. The bubble images from two perpendicular directions are used for determination of rectangles located at edges of the bubble image (Fig.4). Area of those rectangles should satisfy the following inequalities. If the inequalities are not satisfied, the rectangle dimensions must be proportionally increased.

$$\pi \frac{a_x \cdot b_x}{4} \geq S_x \qquad \pi \frac{a_y \cdot b_y}{4} \geq S_y \tag{4}$$

where: S_x i S_y – area calculated from the sum of areas of pixels forming the bubble image

Next, dimensions of ellipses inscribed into the rectangles are defined. Their areas are equal to S_x and S_y, respectively. Dimensions of ellipse semi-axes d_{x1}, d_{x2}, d_{y1}, and d_{y2} are

defined from the Monge circle equation by solution of the following system of equations:

$$\begin{cases} d_{x1}^2 + d_{x2}^2 = \dfrac{a_x^2 + b_x^2}{4} \\ S_x = \pi \cdot d_{x1} d_{x2} \end{cases} \quad \text{and} \quad \begin{cases} d_{y1}^2 + d_{y2}^2 = \dfrac{a_y^2 + b_y^2}{4} \\ S_y = \pi \cdot d_{y1} d_{y2} \end{cases} \tag{5}$$

Coordinates of projections of points of contact *A, B* and *C* of the ellipsoid with rectangles are determined from geometric relations. The coordinates x_A, y_A, z_A, x_B, ,z_A and z_B are calculated by solution of the set of equations:

$$\begin{cases} x_A = X_1 \sin\alpha - Z_1 \cos\alpha \\ x_B = \dfrac{b_x}{2} \\ z_B = X_2 \cos\alpha + Z_2 \sin\alpha \end{cases} \tag{6}$$

$$\begin{cases} y_A = Y_1 \sin\beta - V_1 \cos\beta \\ y_B = \dfrac{b_y}{2} \\ z_C = Y_2 \cos\beta + V_2 \sin\beta \end{cases} \tag{7}$$

$$z_A = \frac{a_x + a_y}{4} \tag{8}$$

where:

$$\begin{cases} \dfrac{X_1^2}{d_{x1}^2} + \dfrac{Z_1^2}{d_{x2}^2} = 1 \\ \dfrac{a_x}{2} = X_1 \sin\alpha + Z_1 \cos\alpha \end{cases} \quad \text{and} \quad \begin{cases} \dfrac{X_2^2}{d_{x1}^2} + \dfrac{Z_2^2}{d_{x2}^2} = 1 \\ \dfrac{b_x}{2} = X_2 \cos\alpha - Z_2 \sin\alpha \end{cases} \tag{9}$$

$$\sin\alpha = \sqrt{\frac{Z_1^2 X_1^2}{Z_1^2 X_1^2 + \left(d_{x1}^2 - X_1^2\right)^2}} \quad \text{and} \quad \cos\alpha = \sqrt{\frac{\left(d_{x1}^2 - X_1^2\right)^2}{Z_1^2 X_1^2 + \left(d_{x1}^2 - X_1^2\right)^2}} \tag{10}$$

On the basis of the defined points of contact of the ellipsoid projection into the planes *XZ* and *YZ* it is possible to determine the remaining coordinates from the ellipsoid projection into the *XY* plane (Fig.6).

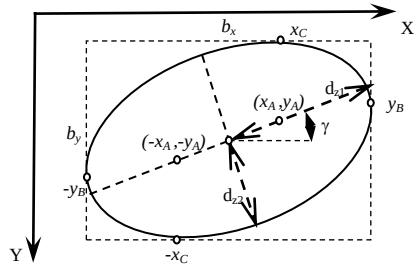

Fig. 6: Ellipsoide projection into *XY* plane

The angle of rotation γ is calculated from:

$$\gamma = arctg \frac{x_A}{y_A} \tag{11}$$

Next, the other coordinates of the point of contact of the ellipsoid x_C, y_B are determined

$$x_C = X_3 \sin\gamma - Y_3 \cos\gamma \quad \text{and} \quad y_B = X_4 \cos\beta + Y_4 \sin\beta \tag{12}$$

where:

$$\begin{cases} \dfrac{X_3^2}{d_{z1}^2} + \dfrac{Y_3^2}{d_{z2}^2} = 1 \\ \dfrac{b_x}{2} = X_3 \sin\gamma + \dfrac{d_{z1}^2 - X_3^2}{X_3} \sin\gamma \end{cases} \tag{13}$$

$$\begin{cases} \dfrac{X_4^2}{d_{z1}^2} + \dfrac{Y_4^2}{d_{z2}^2} = 1 \\ \dfrac{b_y}{2} = X_4 \cos\gamma - Y_4 \sin\gamma \end{cases} \tag{14}$$

$$\sin\gamma = \sqrt{\frac{Y_4^2 X_4^2}{Y_4^2 X_4^2 + \left(d_{z1}^2 - X_4^2\right)^2}} \quad \text{and} \quad \cos\gamma = \sqrt{\frac{\left(d_{z1}^2 - X_4^2\right)^2}{Y_4^2 X_4^2 + \left(d_{z1}^2 - X_4^2\right)^2}} \tag{15}$$

Having all the considered coordinates $A(x_A,y_A,z_A)$, $B(x_B,y_B,z_B)$ and $C(x,,y_C,z_C)$ with the prism of the side dimensions a_x, b_x, b_y, we can determine the ellipsoid diameters d_x, d_y, d_z by solution of the following set of equations:

$$\begin{cases} \dfrac{x_A^2}{d_x^2} + \dfrac{y_A^2}{d_y^2} + \dfrac{z_A^2}{d_z^2} = 1 \\ \dfrac{x_B^2}{d_x^2} + \dfrac{y_B^2}{d_y^2} + \dfrac{z_B^2}{d_z^2} = 1 \\ \dfrac{x_C^2}{d_x^2} + \dfrac{y_C^2}{d_y^2} + \dfrac{z_C^2}{d_z^2} = 1 \end{cases} \tag{16}$$

On this basis an image of the ellipsoid is determined in the 3D space and the bubble volume is calculated.

$$V_p = \tfrac{3}{4}\pi \; d_x d_y d_z \tag{17}$$

4. THE TEST RESULTS

A gas bubble flow was tested in the aeration column in order to estimate correctness of the assumed method. The tests were performed in laboratories. For test purposes a special stand was built (Fig. 7). The stand includes a glass column of 0.2x0.2x1.5m in dimensions *1* supplied from below by replaceable jets *2*. Intensity of the delivered gas *3* is controlled and determined by a rotameter *8*. The bubble column is illuminated by two halogen lamps 150W, emitting visible light *5*. Application of the system of mirrors *4* at the angles 2x45°, 2x22,5° allows to obtain an image consisting of two half-images. The image is registered by a single camera *6*, so it is not necessary to synchronize images from more cameras. The registered particular sequences of the image pass to the computer *7*, with a digital camera with a triple converter CCD produced by CANON MX1. The camera is equipped with a fast interface with a computer IEEE 1394.. Next the images are analyzed in order to determine gas volume fraction in the tested aeration column. Numerical calculations are realized with use of the program VISION and LabView.

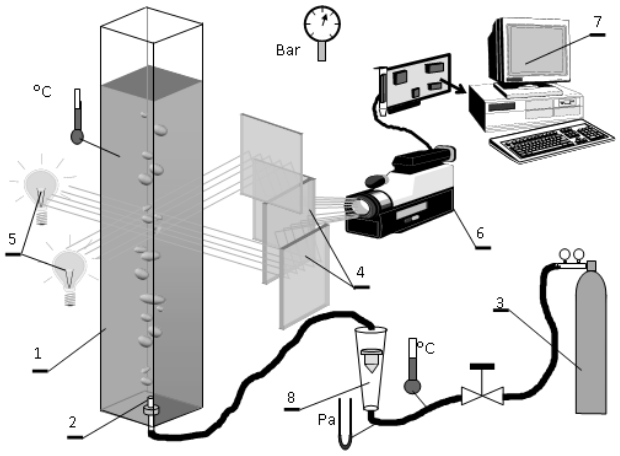

Fig. 7: Test stand

4.1 Test of 3D trajectory rekonstructin

Fig.8 presents results of three-dimensional reconstruction of the bubble flow image for two gas streams. Application of the considered method allows to obtain very distinct images of the flow structures with the measured movement trajectories.

a) b)

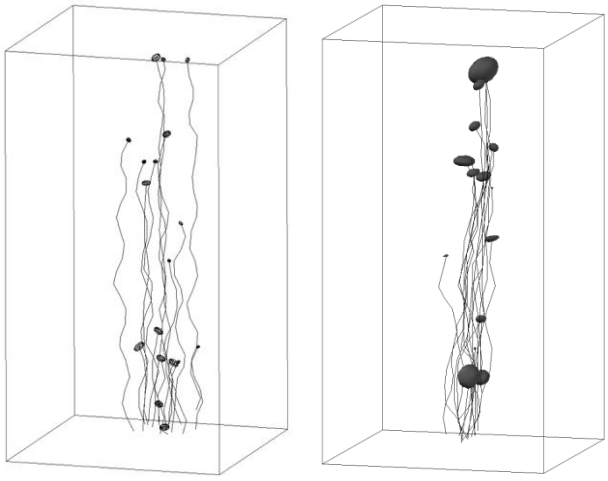

Fig. 8: Reconstruction of the bubble movement trajectory for gas streams a) 0.001 m3/h b) 0.02 m3/h

This method takes into account also shapes and positions of the bubbles, even in the case of very small flows where not all the bubbles preserve spherical shapes. Moreover, movement of such bubbles is realized along the screw line, so their shapes and positions continuously change. The spatial analysis of the flow allows to draw many conclusions concerning behavior of the bubbles, their distribution or processes connected with their circulation while movement which could not be drawn in the case of traditional measurements of two-phase flows. For example, during increase of the gas stream, formation of bubbles of much greater volume is observed, and their shape becomes irregular. Resistances to motion cause high shape deformation although the motion trajectory still preserves its spiral shape. Bubbles can sometimes join or disintegrate. In the case of big streams we can observe formation of the bubble groups. In such groups the bubbles join and divide all the time. Shapes of the bubbles are irregular and they are often subjected to deformations. In the group of big bubbles we can easily find small bubbles the shape of which is similar to a sphere. They usually form as a result of disintegration of bigger bubbles.

The results obtained from the tomograph are parametrized, so it is possible to determine local velocities. It is very important while analysis of the movement trajectory where increase of the gas stream at the initial phase causes limitation of the zone of bubble movement caused by increase of bubble convection by the liquid movement in the bubble core. The bubbles carried away by a liquid are attracted to the stream centre where there is a greater liquid velocity. In the case of continuation of the gas stream increase, the convection zone diameter increases, too.

a) b)

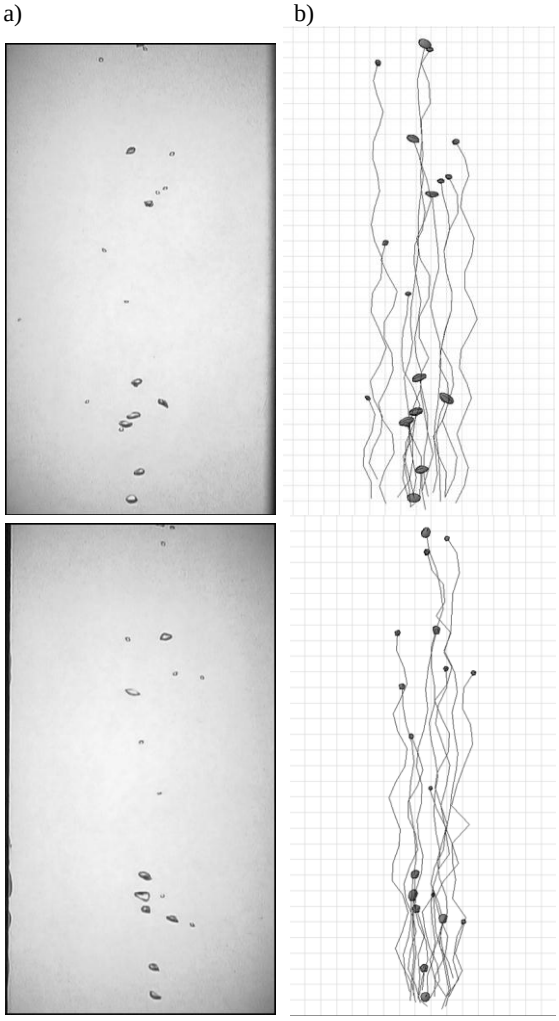

Fig.9. Flow images for gas streams 0.001 m3/h a) image from the camera, b) image from the tomograph.

The reconstruction results were compared with the images obtained from the video camera for the same projection directions, and then the range of applicability of the proposed measuring method was determined. In the case of low values of the gas stream where bubble joining or dividing does not take place very good results are obtained (Fig.9). Some bubbles have a little different shapes than those registered by the camera and it is caused by the shape approximation. However, the results can be treated as

satisfactory. The movement trajectories for particular bubbles prove that there is no interactions (joining or disintegration) between the moving bubbles.

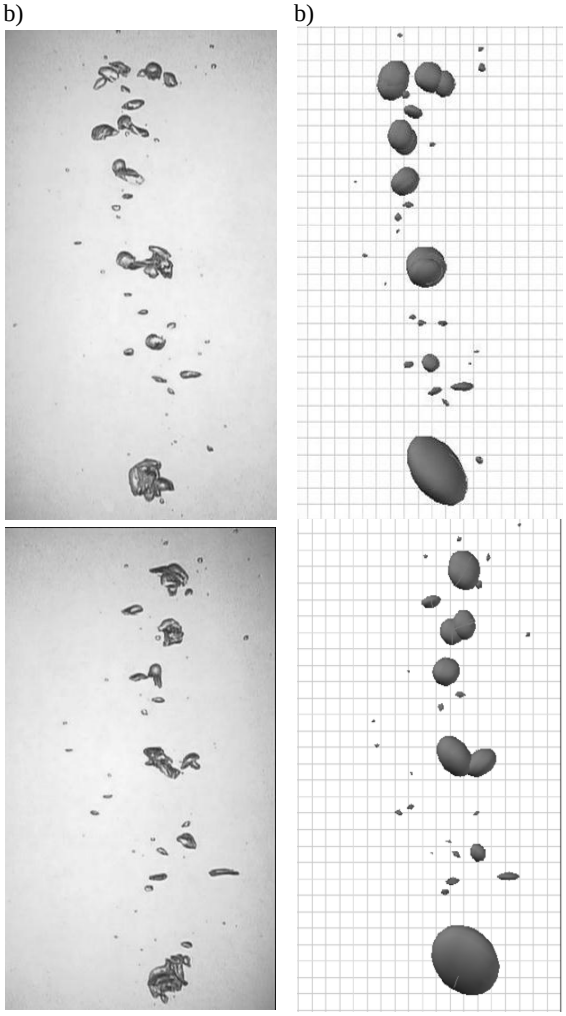

Fig.10. Flow images for gas streams 0.06 m3/h a) image from the camera b) image from the tomograph.

Similar analysis for greater gas streams (Fig.10) gives less satisfactory results. It can be seen that groups of bubbles moving close together are shown as one big bubble. This solution leads to much greater mistakes but it does not mean that the presented method is not suitable for the bubble flow tests. In the case of complex gas-liquid flows, the mistakes of the order of several of even more percents can be sometimes understood as a satisfactory result.

4.2 Tests of the bubble flow

The data obtained from the image tomograph allow to determine parameters describing the aeration process. The bubble movement rate and the bubble volume belong to the most important parameters. Their ratio often allows to optimize the process.

Fig.11 shows the measurement results obtained for mean rates of the bubble movement depending on the bubble volume. Formation of greater bubbles depends on a value of the gas stream flowing from the nozzle. After exceeding a certain critical volume, the bubble movement rate is constant. It is caused by increase of resistances to motion. Let us see a great discrepancy between the rate values for small bubbles. It is caused by strong influence of the surroundings on the small bubble movement rate. A small bubble moving near a big bubble often moves with a similar rate. The zone where a small bubble is moving is also important. Movement of the bubble stream causes the liquid circulation which often strongly influences the movement rate of a small bubble.

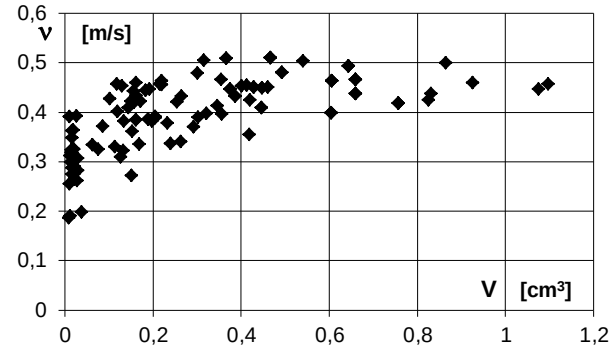

Fig.11. Dependence of the bubble movement rate and the bubble volume

Values of the gas bubble movement rates were compared with the theoretical relationships described in literature [13]. Fig. 12 shows dependence of convection rate for gas bubbles in water of temperature 20°C. Lines 1 and 3 describe the maximum rates of the bubble flow in distilled water. The dashed field expresses the range of experimental data obtained by various authors. It is easy to find that the gas bubble rate in water depends on shapes and dimensions of bubbles and contents of surfactants in water. It was assumed that the diameter of the bubble dbe is the diameter of the sphere volume of which is equal to volume of the bubble approximated by ellipsoid.

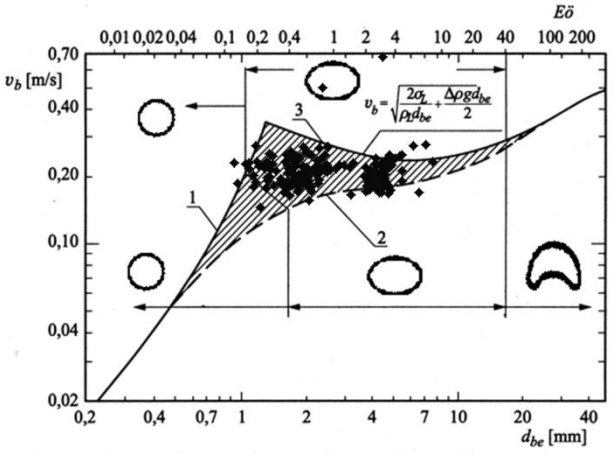

Fig.12. Movement rate of the gas bubbles depending on their diameters [13].

One of the most popular maps of bubble shapes was proposed by Grace, Wairegi and Nguyen [14]. Fig.14 shows comparison of the results from the image tomograph and from theoretical relationships proposed by Grace, Wairegi and Nguyen. In Fig.14 spherical, ellipsoidal and umbrella-shaped bubbles are marked by points of different shapes. The measuring points were re-calculated according to the following relationships.

$$Eo = \frac{g\ (\rho_L - \rho_G) d_{be}^2}{\sigma_L} \tag{18}$$

$$\mathrm{Re} = \frac{v_b d_{be} \rho_L}{\eta_L} \tag{19}$$

$$Mo = \frac{g \eta_L^4 (\rho_L - \rho_G)}{\rho_L^2 \sigma_L^{\ 3}} \tag{20}$$

where: ρ_L ρ_G – density of liquid and gas, g – acceleration of gravity, σ_L – coefficient of the liquid surface tension, v_b – bubble velocity, η_L – coefficient of the liquid absolute viscosity.

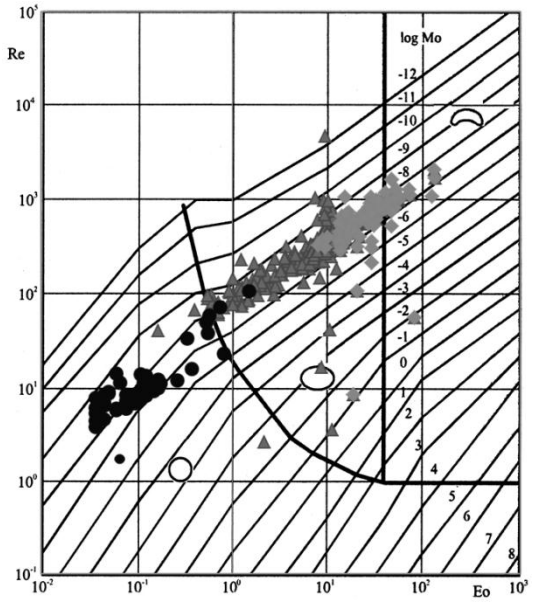

Fig.13. Comparison of the results of bubble shape measurements and the map proposed by Grace, Wairegi and Nguyen [14].

From analysis of the obtained results it appears that there is a good convergence between experimental results and theoretical relationships. Water and air for which the logarithm of the Morton number is 7.5 were used for tests. The most measuring points oscillate around the line corresponding to the value 7.5 at the graph. Also spherical and ellipsoidal bubbles are included in the areas corresponding to theoretical relationships. The umbrella-shaped bubbles are located at the border of the areas. It is caused by difficulties with accurate determination of the bubble shape. Bigger ellipsoidal bubbles undergo deformations while moving. They become plane and take an umbrella-shaped form, after some time they become ellipsoidal again. Thus, it is difficult to classify the bubbles, see the presented characteristic.

5. CONCLUSIONS

The proposed solution using image tomography allows to determine the bubble movement trajectory in the aeration column. Precise determination of the trajectory allows to define the moving bubble local rate. It is a very helpful measuring device used in tests of processes where bubble movement must be known. Comparison of the measured values with widely known relationships proves that conclusions.

Moreover, the three-dimensional image of movement of a group of bubbles allows to analyse the phenomena occurring while movement. It is also possible to determine volume of the moving bubble. We are able to observe changes of the bubble positions and draw conclusions concerning relations between their movement, circulating liquid and other bubbles present in the neighbourhood.

The presented solution is helpful while tests in processing engineering or gas-liquid flows.

REFERENCES

[1] Prosperetti, A. "Bubbles". *Physics of Fluids* no.16, pp.1852-1865, 2004.

[2] Magnaudet, J. & Eames, I. "2000 The motion of high-Reynolds-number bubbles in inhomogeneous flows". *Annual Review of Fluid Mechanics*, vol. 32, pp. 659-708, 2000

[3] Chang M. Y., Moris B.,"Solubilitiea and Mass Transfer Coefficients of Carbon Monoxide in a Gas-Inducing Reactor Operating With Organic Liquids Under High Pressure and Temperatures", *Chemical Engineering Science*, vol 47. No. 13/14, 1992..

[4] Mayinger F., Feldmann, O., "Optical Measurements - Techniques and Applications 2nd Edition", *Heidelberg: Springer*, 2001.

[5] Yonguk R., Kuang-An C., Ho-Joon L., "Use of bubble image velocimetry for measurement of plunging wave impinging on structure and associated greenwater", *Measurement Scince and Technology*; *Institute of Physics Publishing* no16, pp. 1945-1953, 2005

[6] Leifer I., de Leeuw G., Cohen L.H., "Optical Measurement of Bubbles: System Design and Application", *Journal of atmospheric and oceanic technology*, vol. 20, no9, pp. 1317-1332, 2003

[7] Kawaguchi T., Akasaka Y., Maeda M., "Size measurements of droplets and bubbles by advanced interferometric laser imaging technique", *Measurement Scince and Technology*; *Institute of Physics Publishing* no 13, pp. 308-315, 2002.

[8] M.S. Beck and A. Pląskowski, "Cross correlation flowmeters – their design and application", *Adam Hilger, Bristol*, UK, 1987.

[9] Kihm K.D., Ko H.S., Lyons D.P., "Tomographic identification of gas bubbles in two-phase flows with the combined use of the algebraic reconstruction technique and the genetic algorithm. *Optics Letters*, vol. 23, no 9, 1998.

[10] M. R. Rząsa, and A. Pląskowski, "Application of optical tomography for measurements of aeration parameters in large water tanks," Measurement Scince and Technology; *Institute of Physics Publishing* no 14, pp. 199-204, 2003.

[11] Rzasa M. R., "The measuring method for tests of horizontal two-phase gas–liquid flows, using optical and capacitance tomography", *Nuclear Engineering and Design*, Vol.239 no.4, 2009.

[12] Chałubiec J., Rząsa M.R., Dobrowolski B., "Application of image tomography for determination of gas flow parameters in aeration proces", *5th Internation Sympodium on Process Tomography in Poland,* 25-26 August Zakopane 2008

[13] Dziubiński M., Prywer J., „Mechanika płynów dwufazowych", *WNT*, Warszawa 2010

[14] Grace J.R., Wairegi T., *"Properties and Characteristics of drops and bubbles", Encyclopedia of Fluid Mechanics*, Cheremisinoff. Chap 3, gulf Publishing Corporation, Huston, TX., 1986